



The visualized fluorescent probes based on benzothiazole used to detect esterase

Qing Kong, Jing Wang, Yahui Chen, Shiyue Zheng, Xiaoqiang Chen, Yihuan Wang, Fang Wang^{*}

State Key Laboratory of Materials-Oriented Chemical Engineering, College of Chemical Engineering, Jiangsu National Synergetic Innovation Center for Advanced Materials (SICAM), Nanjing Tech University, Nanjing, 211816, China

ARTICLE INFO

Keywords:

Esterase
Fluorescent probes
Benzothiazole-based derivative
Bioimaging
Excited state intramolecular proton transfer

ABSTRACT

Esterase plays a crucial role in regulating various biological activities in living organisms. Detecting esterase levels can be beneficial for the treatment of various diseases. In this study, we have designed and synthesized ESIPT (excited state intramolecular proton transfer)-inspired fluorescent probes **HBT-EA**, **HBT-MA-EA**, and **HBT-Py-EA**, based on benzothiazole derivatives, to detect and identify esterase. All three probes exhibited remarkable enhancement of fluorescent signal in the presence of esterase. These probes were also utilized to detect esterase in living cells with high sensitivity and specificity. Furthermore, a test strips experiment suggests that the probes can recognize esterase accompanied by remarkable color change. Overall, our data suggest that these probes are effective tools for the detection of endogenous esterase, and we expect that they will be further applied in biological and materials science research.

1. Introduction

Esterase is an enzyme that catalyzes the hydrolysis of esters into corresponding alcohols and acids [1,2], which plays an important role in the biological activities of living organisms. Typically, esterase can regulate various metabolic functions, including gene expression, ester metabolism, material transport, and detoxification [3–6], due to its extremely high catalytic turnover rate and substrate specificity [7]. In addition, esterase is also an important drug target and prodrug activator [8–12]. As an important biological metabolic enzyme, its absence or abnormal expression directly contributes to many diseases, such as Wolman disease, obesity, atherosclerosis, cancer, hyperlipidemia, and hepatic steatosis [13–19]. Therefore, the development of novel and effective esterase detection tools is important for biomedical research.

To date, various analysis methods including colorimetry, spectrophotometry, plate assays and chromatography that have been developed to detect esterase [20–23]. However, most of these methodologies are complicated to operate, may cause damage to the organism, and cannot achieve real-time detection. Compared with traditional methods, fluorescent probe method has many advantages, such as low cost, convenient use, high sensitivity and short response time, which can realize real-time non-destructive imaging of esterase [24–29]. Therefore, this method has a wide range of applications in biological imaging [5,

30–33].

The common excited state intramolecular proton transfer (ESIPT) fluorophore 2-(2'-hydroxyphenyl)-benzothiazole (HBT) has been widely used to construct fluorescent probes due to its large Stokes shift, high fluorescence quantum yield and high photostability [34–37]. Benzothiazole derivatives also have excellent optical properties due to their large, conjugated rigid plane and delocalized π bonds; at the same time, they display aggregation-induced emission (AIE) properties, and therefore fluorescence actually increases at high concentrations as in an aggregate or solid state [38–41]. This feature compensates for the shortcomings of previous probes, and therefore benzothiazole derivatives are more widely used in the field of biomaterials.

In this study, we designed and synthesized multicolor fluorescent probes based on benzothiazole (**HBT-EA**, **HBT-MA-EA**, **HBT-Py-EA**), and used these probes to detect esterase. As shown in [Scheme 1](#), the ester-protected hydroxyl group of these probes is converted into a hydroxyl group via hydrolysis catalyzed by esterase, resulting in the release of the fluorescent signal. It is worth mentioning that acetoxymethyl (AM) ether was used as the recognition group, which releases formaldehyde (FA) upon enzyme digestion, which can also be used as a signal molecule to judge the degree of cell healing [42].

^{*} Corresponding author.

E-mail address: fangwang@njtech.edu.cn (F. Wang).

2. Experimental section

2.1. Materials and equipment

In the absence of specific instructions, all chemicals used in the experiment are purchased on the market and need not be further purified. Mass spectra were obtained from Q-ToF mass spectrometer (Agilent 1260). ^1H NMR and ^{13}C NMR spectra were obtained using Bruker spectroscopy (Bruker 400 MHz). UV-vis absorption spectra were carried out on α -1860A UV/vis spectrophotometer. Fluorescence emission spectra were collected using RF-5301/PC fluorophotometer (SHIMADZU). The cells were imaged by fluorescence microscopy (OLYMPUS IX73).

2.2. Synthesis

The synthesis routes of the probes are shown in Scheme 2. Compounds **HBT**, **HBT-MA**, **HBT-Py** have been synthesized by the previously reported literature [43].

HBT: ^1H NMR (DMSO- d_6 , 400 MHz), δ (ppm): 11.36 (1H, s), 8.13 (1H, d, $J = 5.9$ Hz), 8.05 (1H, d, $J = 6.1$ Hz), 7.99 (1H, s), 7.54 (1H, t, $J = 5.7$ Hz), 7.45 (1H, t, $J = 5.7$ Hz), 7.22 (1H, d, $J = 6.2$ Hz), 6.98 (1H, d, $J = 6.2$ Hz), 2.33 (3H, s); ^{13}C NMR (DMSO- d_6 , 100 MHz), δ (ppm): 165.94, 154.84, 152.11, 134.90, 133.89, 129.07, 128.93, 127.09, 125.67, 122.70, 122.63, 118.58, 117.53, 20.68. LC-MS (ESI): m/z [M + H] $^+$ calculated for $\text{C}_{14}\text{H}_{11}\text{NOS}$: 242.0640; found: 242.0572.

HBT-MA: ^1H NMR (DMSO- d_6 , 400 MHz), δ (ppm): 12.76 (1H, s), 10.33 (1H, s), 8.21 (1H, d, $J = 3.2$ Hz), 8.11 (2H, d, $J = 6.1$ Hz), 7.73 (1H, s), 7.60 (1H, t, $J = 5.7$ Hz), 7.52 (1H, t, $J = 5.7$ Hz), 2.34 (1H, s); ^{13}C NMR (DMSO- d_6 , 100 MHz), δ (ppm): 192.30, 165.67, 157.53, 151.49, 135.76, 134.04, 133.58, 129.78, 127.43, 126.32, 123.73, 122.79, 122.76, 119.60, 20.22. LC-MS (ESI): m/z [M + H] $^+$ calculated for $\text{C}_{15}\text{H}_{11}\text{NO}_2\text{S}$: 270.0589; found: 270.0513.

HBT-Py: ^1H NMR (DMSO- d_6 , 400 MHz), δ (ppm): 13.13 (1H, s), 8.87 (2H, d, $J = 4.7$ Hz), 8.25 (3H, d, $J = 5.1$ Hz), 8.17 (1H, s), 8.13 (1H, d, $J = 4.5$ Hz), 7.83 (1H, s), 7.79 (1H, s), 7.70 (1H, s), 7.64 (1H, t, $J = 6.5$ Hz), 7.56 (1H, d, $J = 5.7$ Hz), 4.30 (3H, s), 2.42 (3H, s); ^{13}C NMR (DMSO- d_6 , 100 MHz), δ (ppm): 168.76, 154.47, 153.10, 151.30, 145.62, 135.30, 133.02, 132.91, 131.20, 129.63, 127.67, 126.58, 125.01, 124.13, 124.01, 122.95, 122.46, 117.67, 47.40, 20.44. LC-MS (ESI): m/z [M] $^+$ calculated for $\text{C}_{22}\text{H}_{19}\text{N}_2\text{OS}^+$: 359.1218; found: 359.1176.

2.2.1. Synthesis of compound **HBT-EA**

Compound **HBT** (0.64 g, 2.66 mmol), bromomethyl acetate (0.61 g, 4.00 mmol) and Cs_2CO_3 (0.87 g, 2.66 mmol) were dissolved in anhydrous DMF (25 mL) under nitrogen protection. The mixture was stirred at room temperature for 24 h under exclusion of light. After the reaction was completed, water (100 mL) was slowly added and stirred for 5 h to produce the white precipitation. Then the precipitation was collected, washed with water several times, and dried to obtain a white solid crude

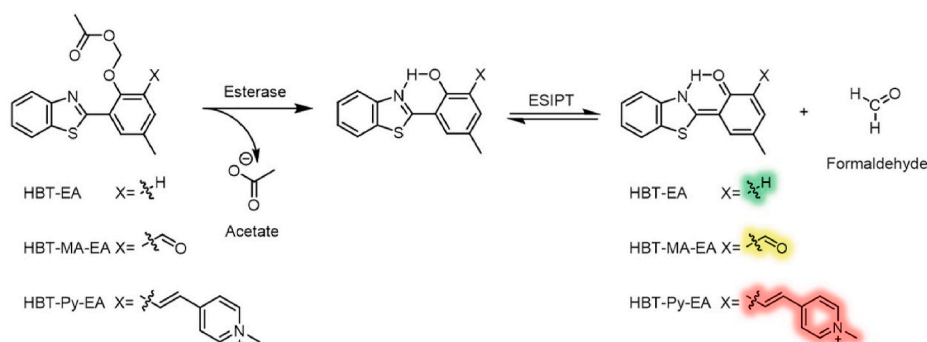
product. Finally, the crude product was purified by column chromatography to obtain the pure white solid product **HBT-EA** (0.75 g, 90%). The synthesized **HBT-EA** was characterized by ^1H NMR, ^{13}C NMR and electrospray ionization-mass spectrometry (ESI-MS) (Fig. S1-S3). ^1H NMR (DMSO- d_6 , 400 MHz), δ (ppm): 8.25 (1H, s), 8.14 (1H, d, $J = 8.0$ Hz), 8.05 (1H, d, $J = 8.0$ Hz), 7.54 (1H, t, $J = 6.8$ Hz), 7.45 (1H, t, $J = 7.2$ Hz), 7.38 (1H, d, $J = 8.4$ Hz), 7.32 (1H, d, $J = 8.0$ Hz), 5.99 (2H, s), 2.38 (3H, s), 2.08 (3H, s). ^{13}C NMR (DMSO- d_6 , 100 MHz), δ (ppm): 169.44, 161.91, 152.13, 151.53, 135.45, 132.82, 132.13, 128.99, 126.29, 125.07, 122.48, 122.02, 121.83, 115.50, 85.10, 20.60, 20.09. LC-MS (ESI): m/z [M + H] $^+$ calculated for $\text{C}_{18}\text{H}_{15}\text{NO}_3\text{S}^+$: 314.0851; found: 314.0832.

2.2.2. Synthesis of compound **HBT-MA-EA**

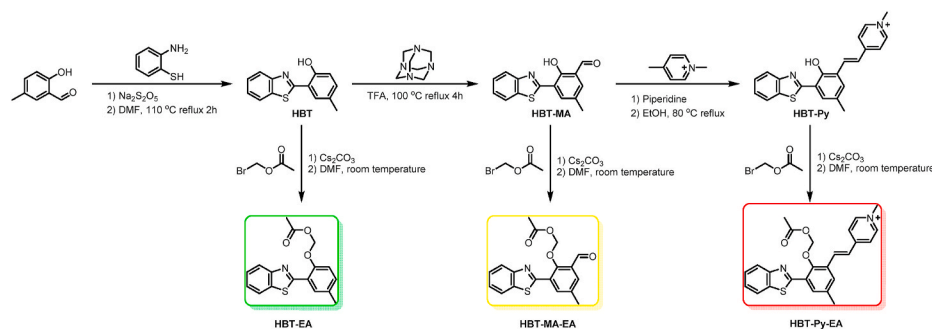
Compound **HBT-MA** (1.17 g, 4.35 mmol), bromomethyl acetate (1.00 g, 6.52 mmol) and Cs_2CO_3 (1.42 g, 4.35 mmol) were dissolved in anhydrous DMF (40 mL) under nitrogen protection. The mixture was stirred at room temperature for 24 h under exclusion of light. After the reaction was completed, water (100 mL) was slowly added and stirred for 2 h to produce the white precipitation. Then the precipitation was collected, washed with water several times, and dried to obtain a white solid crude product. Finally, the crude product was purified by column chromatography to obtain the pure white solid product **HBT-MA-EA** (0.88 g, 59%). The synthesized **HBT-MA-EA** was characterized by ^1H NMR, ^{13}C NMR and electrospray ionization-mass spectrometry (ESI-MS) (Fig. S4-S6). ^1H NMR (DMSO- d_6 , 400 MHz), δ (ppm): 10.23 (1H, s), 8.41 (1H, s), 8.19 (1H, d, $J = 8.0$ Hz), 8.12 (1H, d, $J = 8.0$ Hz), 7.81 (1H, s), 7.59 (1H, d, $J = 8.0$ Hz), 7.51 (1H, d, $J = 8.0$ Hz), 5.74 (2H, s), 2.47 (3H, s), 1.81 (3H, s). ^{13}C NMR (DMSO- d_6 , 100 MHz), δ (ppm): 189.60, 169.23, 161.33, 154.04, 151.79, 135.70, 135.66, 135.41, 131.91, 129.89, 127.31, 126.62, 125.73, 122.94, 122.10, 90.19, 20.14, 20.12. LC-MS (ESI): m/z [M + H] $^+$ calculated for $\text{C}_{18}\text{H}_{16}\text{NO}_4\text{S}^+$: 342.0800; found: 342.0678.

2.2.3. Synthesis of compound **HBT-Py-EA**

Compound **HBT-MA** (0.20 g, 0.56 mmol), bromomethyl acetate (0.13 g, 0.84 mmol) and Cs_2CO_3 (0.18 g, 0.56 mmol) were dissolved in anhydrous DMF (15 mL) under nitrogen protection. The mixture was stirred at room temperature for 24 h under exclusion of light. After the reaction was completed, the solution was extracted with H_2O and CH_2Cl_2 several times, and the organic phase was taken out and dried to obtain a yellow crude product. Finally, the crude product was purified by column chromatography to obtain pure yellow solid product **HBT-Py-EA** (0.75 g, 31%). The synthesized **HBT-Py-EA** was characterized by ^1H NMR, ^{13}C NMR and electrospray ionization-mass spectrometry (ESI-MS) (Fig. S7-S9). ^1H NMR (DMSO- d_6 , 400 MHz), δ (ppm): 8.91 (2H, d, $J = 4.0$ Hz), 8.29 (2H, d, $J = 8.0$ Hz), 8.19 (2H, t, $J = 8.0$ Hz), 8.11 (2H, t, $J = 8.0$ Hz), 7.94 (1H, s), 7.62 (1H, d, $J = 12.0$ Hz), 7.59 (1H, t, $J = 8.0$ Hz), 7.51 (1H, t, $J = 8.0$ Hz), 5.65 (2H, s), 4.29 (3H, s), 2.48 (3H, s), 1.69 (3H, s). ^{13}C NMR (DMSO- d_6 , 100 MHz), δ (ppm): 169.37, 162.12,



Scheme 1. The molecular structures and response mechanism of probes for specific detection of esterase.



Scheme 2. Synthesis of probe HBT-EA, HBT-MA-EA, HBT-Py-EA.

151.97, 151.87, 150.96, 145.35, 135.52, 135.42, 133.80, 131.86, 130.29, 129.86, 127.23, 126.58, 125.66, 123.86, 122.90, 122.06, 89.61, 47.08, 20.38, 20.25. LC-MS (ESI): m/z [M]⁺ calculated for C₂₅H₂₃N₂O₃S⁺: 431.1424; found: 431.1395.

2.3. Preparation of samples and test solution

Stock solutions of each probe (1 mM) were prepared in DMSO. Porcine liver esterase stock solution (20 U/mL) was freshly prepared with ultrapure water. Various ion (10 mM), amino acid (10 mM), and enzyme (20 U/mL) solutions were prepared using ultrapure water. The probe solutions for in living cells experiments were prepared using on biological-grade DMSO. Stock solutions were diluted with phosphate-buffered saline (10 mM, pH = 7.4) to obtain test solutions. The test solutions used in experiments were all prepared from the same batch of samples, which were stored in a refrigerator at 2 °C, and were kept at room temperature prior to use.

2.4. Calculation of the limit of detection (LOD)

The limit of detection (LOD) was calculated according to the following equation (1):

$$\text{LOD} = 3 \sigma/m \quad (1)$$

where σ represents the standard deviation of the blank sample ($n = 11$), and m represents the slope of the linear fit equation.

2.5. Cells culture and imaging

HeLa cells were cultured in T25 culture dishes containing Dulbecco's modified Eagle Medium (DMEM) containing 10% fetal bovine serum and 1% penicillin. The temperature of the incubator was maintained at 37 °C and the CO₂ concentration at 5%.

Cells were pre-transferred to culture dishes and then incubated for 20 h. Two groups were studied as follows: (1) HeLa cells were incubated with probes HBT-EA, HBT-MA-EA, HBT-Py-EA (20 μ M) for 3 h (2) HeLa cells were pre-treated with bis(4-nitrophenyl) phosphate (BNPP, 20 μ M) for 1 h and then incubated with probes HBT-EA, HBT-MA-EA, HBT-Py-EA (20 μ M) for 3 h. Cell imaging was carried out after washing the cells by PBS buffer (pH = 7.4). Fluorescence microscopy was used to image cells. The fluorescence wavelengths were fixed in the green and red channels.

3. Results and discussion

3.1. Molecular design and synthesis

HBT is a typical fluorophore with green fluorescence emission in keto form after photoexcitation, and the strong intramolecular H-bond plays crucial role in fluorescence performance. Upon substituting the hydrogen atom electrophilic substitution reaction, the weak enol form

emission is observed due to the ESIPT process is suppressed. Based on the strategy, we designed and synthesized the esterase-specific probes HBT-EA, HBT-MA-EA and HBT-Py-EA. Besides, probes HBT-MA-EA and HBT-Py-EA exhibit red-shift fluorescence behavior due to the extended π -conjugated system is introduced into ortho-position of hydroxyl group. Moreover, considering the small size of esterase, the steric hindrance effect is negligible with the modification of aldehyde and pyridinium salt groups at ortho-position of hydroxyl group, which indicates that probes HBT-EA, HBT-MA-EA and HBT-Py-EA will present high sensitivity to esterase.

We obtained the pure products HBT-EA, HBT-MA-EA, HBT-Py-EA through the above synthesis routes, all resulting products were confirmed and characterized by NMR and high-resolution mass spectroscopy (Fig. S1-S9).

3.2. Fluorescence assay

We initially explored the fluorescence properties of the newly developed probes HBT-EA, HBT-MA-EA, and HBT-Py-EA. As shown in Fig. 1a, probe HBT-EA (10 μ M) exhibited a weak blue fluorescence around 380 nm in the absence of esterase. As expected, upon addition of esterase (0–0.20 U/mL), a remarkable dark green fluorescence was observed accompanied by the disappearance of the weak blue fluorescence. The fluorescence intensity reached a maximum at 0.16 U/mL esterase, and a 500-fold increase in fluorescence intensity was observed at 527 nm.

By the same principle, as shown in Fig. 1b, probe HBT-MA-EA (10 μ M) exhibited no fluorescence in the absence of esterase, and upon addition of esterase (0–0.20 U/mL), a light green fluorescence was observed. The maximum fluorescence intensity at 542 nm was reached when the concentration of esterase reached 0.20 U/mL. However, it is worth noting that compared with probe HBT-EA, the quantum fluorescence yield of probe HBT-MA-EA after digestion was lower. HBT-MA-EA also decomposed slowly over time in PBS buffer, which emitted some fluorescence at 542 nm.

As shown in Fig. 1c, upon adding esterase (0–0.20 U/mL) to probe HBT-Py-EA, a remarkable red fluorescence was observed. The fluorescence intensity reached a maximum, 8-fold higher than baseline, at 614 nm when the concentration of esterase reached 0.20 U/mL.

Next, we calculated the limit of detection (LOD) of HBT-EA and HBT-Py-EA using equation (1). As shown in Fig. S11, within a certain range, the fluorescence intensity and the esterase concentration show a good linear relationship. We detected the fluorescence of HBT-EA within the esterase concentration range of 0–0.04 U/mL, and fluorescence of HBT-Py-EA within the esterase concentration range of 0–0.048 U/mL. The limits of detection ($3 \sigma/m$) were calculated to be 1.22×10^{-4} U/mL and 1.50×10^{-3} U/mL, respectively.

Finally, we conducted an experiment using an inhibitor of esterase, bis(4-nitrophenyl) phosphate (BNPP) [44]. After incubating esterase (0.20 U/mL) with different concentrations of BNPP (0 μ M, 0.50 μ M, 2.50 μ M, and 5.00 μ M) at 37 °C in a water bath for 30 min, the probe

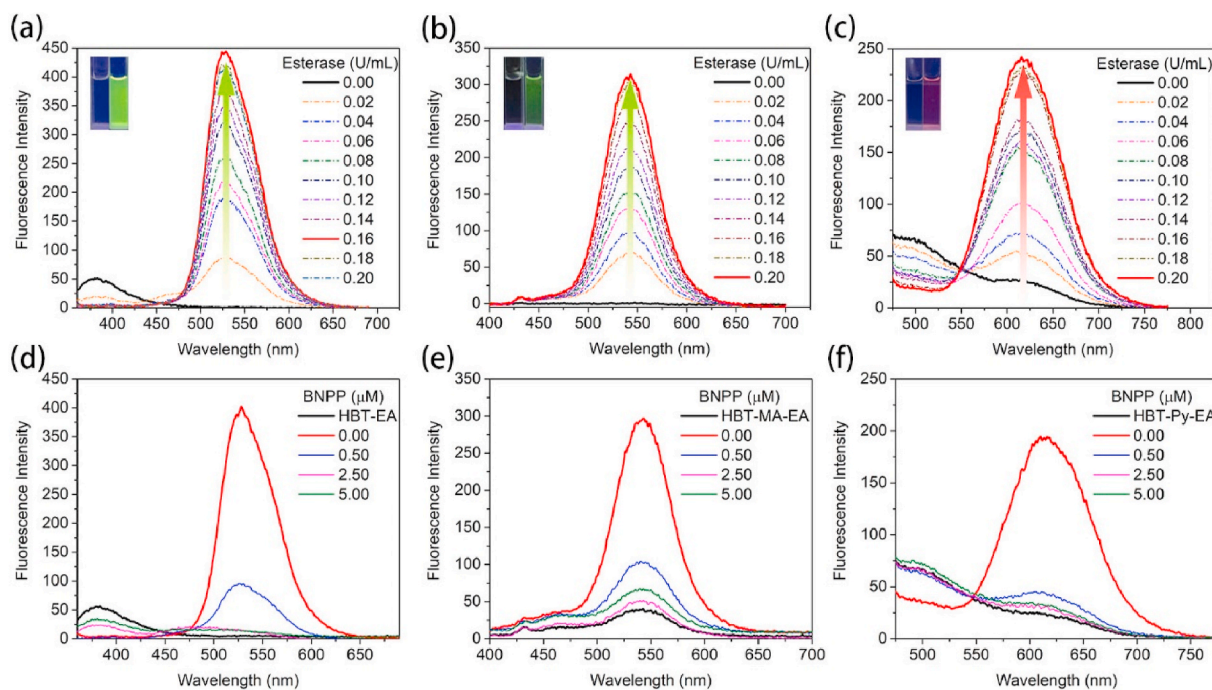


Fig. 1. Changes in fluorescence spectra of (a) **HBT-EA** (10 μM ; $\lambda_{\text{ex}} = 350 \text{ nm}$; Slit: 3 nm/5 nm), (b) **HBT-MA-EA** (10 μM ; $\lambda_{\text{ex}} = 375 \text{ nm}$; Slit: 5 nm/5 nm) and (c) **HBT-Py-EA** (10 μM ; $\lambda_{\text{ex}} = 400 \text{ nm}$; Slit: 10 nm/10 nm) with various esterase concentrations (0–0.2 U/mL) in PBS buffer (10 mM, pH 7.4) at room temperature. Changes in fluorescence spectra of (d) **HBT-EA**, (e) **HBT-MA-EA** and (f) **HBT-Py-EA** in the presence of different concentrations (0–5.00 μM) of BNPP and 0.20 U/mL esterase in PBS buffer (10 mM, pH 7.4) at room temperature.

solutions (10 μM) were added and allowed to react at room temperature for 20 min, and then fluorescence intensity was measured. As shown in Fig. 1d–f, it can be clearly seen that the fluorescence was significantly decreased in the presence of BNPP. When the concentration of BNPP reached 2.5 μM or more, there was almost no fluorescence emitted, indicating that the esterase activity was almost completely inhibited. This indicates that BNPP has a strong inhibitory effect on esterase in this experimental system, and BNPP may also be applied in subsequent intracellular esterase inhibition experiments.

3.3. Selectivity of fluorescent probes

To evaluate the selectivity of **HBT-EA**, **HBT-MA-EA**, and **HBT-Py-EA** towards esterase, we added various common enzymes (acetyl cholinesterase, carbonic anhydrase I, xanthine oxidase, peroxidase, inorganic pyrophosphatase), common amino acids and peptide (Cys, GSH, Hcy), and common ions (K^+ , Na^+ , CO_3^{2-} , SO_3^{2-} , Cl^- , ClO^- , S^{2-}) to the probe

solutions, which were incubated at room temperature prior to measurement of fluorescence. We found that none of these various enzymes, amino acids and peptide, or ions had any significant effect on the fluorescence of the probes (Fig. 2). The histogram of the selectivity of each species is shown in Fig. S12. These data indicated that these three probes possessed relatively high selectivity for esterase compared to other common biological species.

3.4. The effect of pH on fluorescence

In order to evaluate the effects of pH on the developed probes, we added probes and esterase to PBS buffer at different pH values, incubated them at room temperature for 20 min, and then measured fluorescence emission.

HBT-EA demonstrated the best response to esterase at pH 7 (Fig. 3). However, in the acidic or alkali environments of pH 2 ($\lambda_{\text{em}} = 442 \text{ nm}$) and pH 10 ($\lambda_{\text{em}} = 478 \text{ nm}$), the blue fluorescence shifted, potentially as a

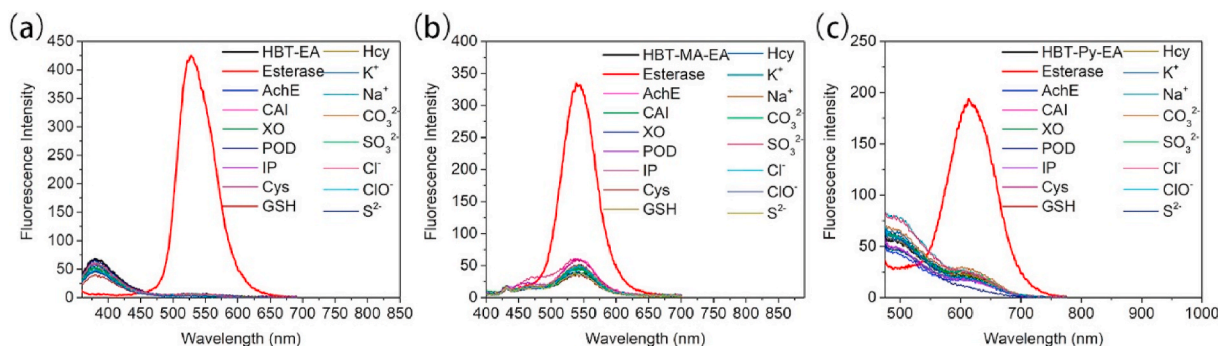


Fig. 2. Fluorescence spectra of (a) **HBT-EA** (10 μM ; $\lambda_{\text{ex}} = 350 \text{ nm}$; Slit: 3 nm/5 nm), (b) **HBT-MA-EA** (10 μM ; $\lambda_{\text{ex}} = 375 \text{ nm}$; Slit: 5 nm/5 nm), (c) **HBT-Py-EA** (10 μM ; $\lambda_{\text{ex}} = 400 \text{ nm}$; Slit: 10 nm/10 nm) in response to esterase (0.20 U/mL) and various other common species in PBS buffer (10 mM, pH 7.4) at room temperature, including: acetyl cholinesterase (AChE), carbonic anhydrase I (CAI), xanthine oxidase (XO), peroxidase (POD), inorganic pyrophosphatase (IP), Cys, GSH, Hcy, K^+ , Na^+ , CO_3^{2-} , SO_3^{2-} , Cl^- , ClO^- and S^{2-} (enzymes at 0.20 U/mL, amino acids and peptide at 10 μM , ions at 10 μM).

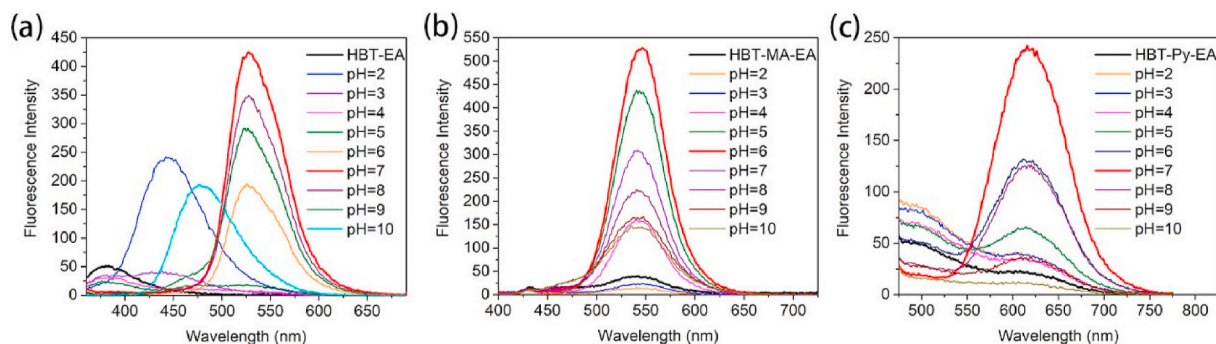


Fig. 3. Fluorescence spectra of (a) HBT-EA, (b) HBT-MA-EA and (c) HBT-Py-EA with 0.20 U/mL esterase in PBS buffer at different pH value (pH = 2–10).

result of changes in molecular configuration. The probe **HBT-MA-EA** displayed the strongest fluorescence response to esterase at pH 6, and the fluorescence intensity decreased in other pH environments. Similarly, the probe **HBT-Py-EA** responded best to esterase at pH 7, and the fluorescence at 614 nm was quenched in over-acidic or over-alkali environments.

The above results indicated that the probes can be applied for esterase detection at biological pH levels.

3.5. Cell imaging experiments

As mentioned above, these probes may be applied to detect esterase activity in living cells. We added the probes (20 μ M) to HeLa cell cultures and incubated them for 3 h, then analyzed fluorescence via imaging on a fluorescence microscope. Dark green fluorescence appeared when the cells were incubated for 3 h with **HBT-EA** (Fig. 4a, d), light green fluorescence appeared when the cells were incubated for 3 h with **HBT-MA-EA** (Fig. 4b, e), and red fluorescence appeared when the cells were incubated for 3 h with **HBT-Py-EA** (Fig. 4c, f). This fluorescence emission was caused by the formation of hydroxyl groups by endogenous esterase hydrolysis of the probe, indicating that the probes can be applied to detect the esterase activity in living cells.

In addition, HeLa cells were pretreated with BNPP (20 μ M) for 1 h, and then incubated with probes for 3 h to confirm probe function. Cells without inhibitor pretreatment still showed obvious fluorescence, while cells pretreated with BNPP displayed a significant decrease in fluorescence intensity (Fig. 4g–l).

The above results indicated that **HBT-EA**, **HBT-MA-EA** and **HBT-Py-EA** can be used to specifically image endogenous esterase in living cells, and esterase inhibitors effectively inhibit this fluorescence emission.

3.6. On-site analysis

For convenient use in on-site visual screening analyses, we constructed portable filter paper strips for esterase detection. First, the test paper was soaked in a solution containing the fluorescent probes (1 mM, CH₃CN), then was naturally dried. The test papers were then treated with an esterase solution (20 U/mL, H₂O), and irradiated with an ultraviolet lamp after 40 min. It was clearly observed that the probes exhibited light blue fluorescence prior to esterase treatment, and following treatment with esterase emitted dark green (**HBT-EA**), light green (**HBT-MA-EA**) and red (**HBT-Py-EA**) fluorescence (Fig. 5). These results demonstrate the convenient application of **HBT-EA**, **HBT-MA-EA** and **HBT-Py-EA** in the visual detection of esterase and provide probes

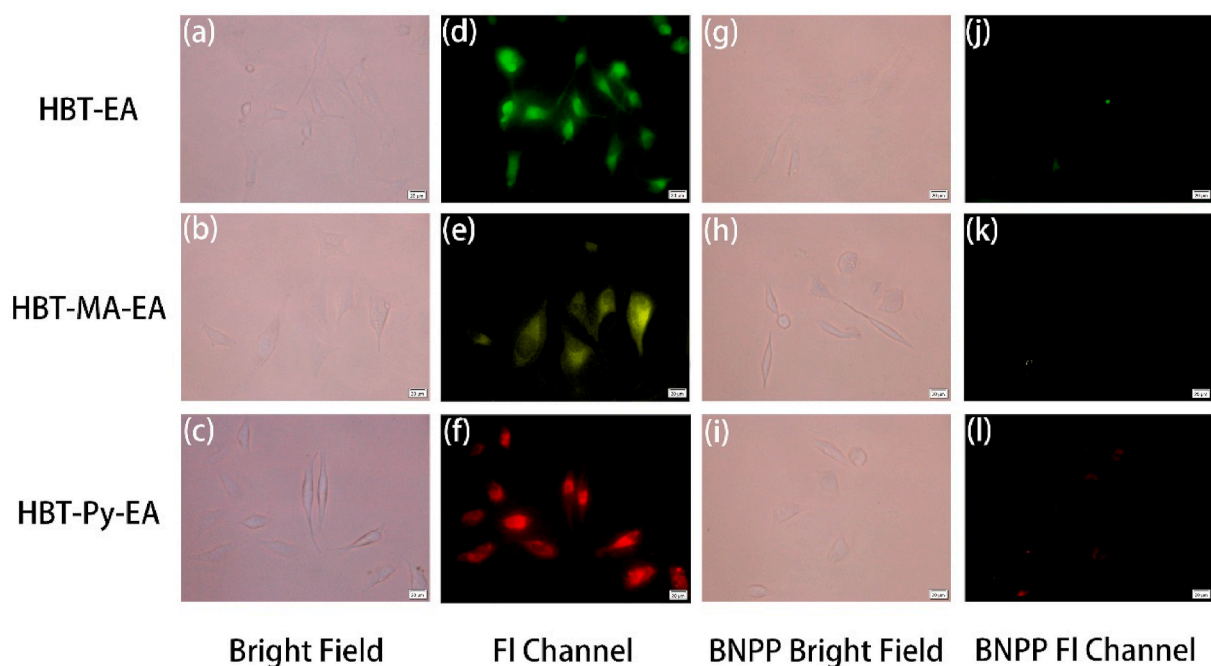


Fig. 4. Bright field and fluorescence microscopy images of HeLa cells incubated with fluorescent esterase probes. (a–f) HeLa cells incubated with **HBT-EA** (20 μ M), **HBT-MA-EA** (20 μ M) and **HBT-Py-EA** (20 μ M) for 3 h. (g–l) HeLa cells incubated with BNPP (20 μ M) for 1 h followed by incubation with **HBT-EA** (20 μ M), **HBT-MA-EA** (20 μ M) and **HBT-Py-EA** (20 μ M) for 3 h.

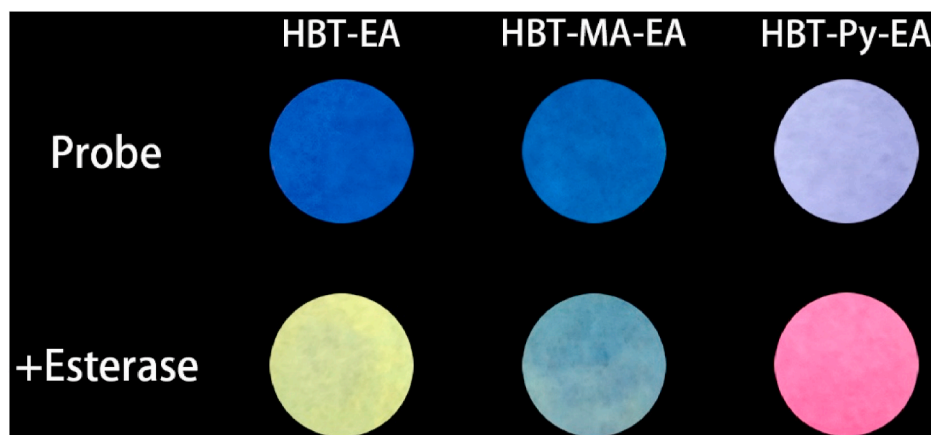


Fig. 5. Images of test strips loaded with probe HBT-EA, HBT-MA-EA and HBT-Py-EA and tested with esterase. Images were taken under irradiation by 365 nm UV light.

with different fluorescence emission to choose.

4. Conclusions

In summary, we designed and synthesized novel fluorescent probes based on benzothiazole derivatives to detect esterase with high sensitivity and good selectivity. The probes exhibited significantly increased fluorescence intensity in the presence of esterase. Importantly, the probes were proven to be suitable for applications under physiological pH conditions. In addition, this series of probes are more suitable for detecting and imaging endogenous esterase in biological environments. Finally, multicolor esterase fluorescent probes also provide a convenient and efficient way for on-site test paper detection of esterase. The above data suggests that these probes have potential value and broad prospects in the fields of materials science and biological research.

Funding

This work was supported by the National Natural Science Foundation of China (21978131 and 21878156); the Six Talent Peaks Project in Jiangsu Province (XCL034); the National Key Research and Development Program of China (2018YFA0902200) and the Project of Priority Academic Program Development of Jiangsu Higher Education Institutions (PAPD).

CRediT authorship contribution statement

Qing Kong: Carried out main laboratory research, and wrote draft of manuscript. **Jing Wang:** Carried out laboratory research of helping synthesis the compounds in this work. **Yahui Chen:** Provided laboratory guidance and revised the manuscript. **Shiyue Zheng:** Carried out laboratory research of cell experiments in this work. **Xiaoqiang Chen:** Provided theoretical guidance. **Yihuan Wang:** Carried out laboratory research of cell experiments in this work. **Fang Wang:** Provided laboratory guidance and revised the manuscript.

Declaration of competing interest

The authors declare that they have no known competing financial interests or personal relationships that could have appeared to influence the work reported in this paper.

Acknowledgments

This study is supported by the National Natural Science Foundation of China (21978131 and 21878156), the Six Talent Peaks Project in

Jiangsu Province (XCL034), the National Key Research and Development Program of China (2018YFA0902200) and the Project of Priority Academic Program Development of Jiangsu Higher Education Institutions (PAPD).

Appendix A. Supplementary data

Supplementary data to this article can be found online at <https://doi.org/10.1016/j.dyepig.2021.109349>.

References

- [1] Beharry AA, Woolley GA. Azobenzene photoswitches for biomolecules. *Chem Soc Rev* 2011;40(8):4422–37.
- [2] Szymanski W, Beierle JM, Kistemaker HAV, Velema WA, Feringa BL. Reversible photocontrol of biological systems by the incorporation of molecular photoswitches. *Chem Rev* 2013;113(8):6114–78.
- [3] Mutch E, Nave R, McCracken N, Zech K, Williams FM. The role of esterases in the metabolism of ciclesonide to desisobutryl-ciclesonide in human tissue. *Biochem Pharmacol* 2007;73(10):1657–64.
- [4] Creighton J, Zhu B, Alexeyev M, Stevens T. Spectrin-anchored phosphodiesterase 4D4 restricts cAMP from disrupting microtubules and inducing endothelial cell gap formation. *J Cell Sci* 2008;121(1):110–9.
- [5] Wang J, Teng Z, Cao T, Qian J, Zheng L, Cao Y, et al. Turn-on visible and ratiometric near-infrared fluorescent probes for distinction endogenous esterases and chymotrypsins in live cells. *Sens Actuators, B* 2020:306.
- [6] Wang J, Teng Z, Zhang L, Yang Y, Qian J, Cao T, et al. Multifunctional near-infrared fluorescent probes with different ring-structure trigger groups for cell health monitoring and in vivo esterase activity detection. *ACS Sens* 2020;5(10):3264–73.
- [7] Zhou H, Tang J, Zhang J, Chen B, Kan J, Zhang W, et al. A red lysosome-targeted fluorescent probe for carboxylesterase detection and bioimaging. *J Mater Chem B* 2019;7(18):2989–96.
- [8] Munoz-Torrero D. Acetylcholinesterase inhibitors as disease-modifying therapies for Alzheimer's disease. *Curr Med Chem* 2008;15(24):2433–55.
- [9] Lavis LD. Ester bonds in prodrugs. *ACS Chem Biol* 2008;3(4):203–6.
- [10] Ji C, Miller MJ. Chemical syntheses and in vitro antibacterial activity of two desferrioxamine B-ciprofloxacin conjugates with potential esterase and phosphatase triggered drug release linkers. *Bioorg Med Chem* 2012;20(12):3828–36.
- [11] Ni M, Zeng WJ, Xie X, Chen ZL, Wu H, Yu CM, et al. Intracellular enzyme-activatable prodrug for real-time monitoring of chlorambucil delivery and imaging. *Chin Chem Lett* 2017;28(6):1345–51.
- [12] Han X, Cheng K, Xu Y, Wang Y, Mm H, Zhang Y, et al. Modularly designed peptide nanoprodrug augments antitumor immunity of PD-L1 checkpoint blockade by targeting indoleamine 2,3-dioxygenase. *J Am Chem Soc* 2020;142(5):2490–6.
- [13] Feng L, Liu ZM, Hou J, Lv X, Ning J, Ge GB, et al. A highly selective fluorescent ES IPT probe for the detection of Human carboxylesterase 2 and its biological applications. *Biosens Bioelectron* 2015;65:9–15.
- [14] Kim S, Kim H, Choi Y, Kim Y. A new strategy for fluorogenic esterase probes displaying low levels of non-specific hydrolysis. *Chem Eur J* 2015;21(27):9645–9.
- [15] Peng L, Xu S, Zheng X, Cheng X, Zhang R, Liu J, et al. Rational design of a red-emissive fluorophore with AIE and ES IPT characteristics and its application in light-up sensing of esterase. *Anal Chem* 2017;89(5):3162–8.
- [16] Zhang Y, Chen W, Feng D, Shi W, Li X, Ma H. A spectroscopic off-on probe for simple and sensitive detection of carboxylesterase activity and its application to cell imaging. *Analyst* 2012;137(3):716–21.

- [17] Wang X, Liu H, Li J, Ding K, Lv Z, Yang Y, et al. A fluorogenic probe with aggregation-induced emission characteristics for carboxylesterase assay through formation of supramolecular microfibers. *Chem Asian J* 2014;9(3):784–9.
- [18] Li D, Li Z, Chen W, Yang X. Imaging and detection of carboxylesterase in living cells and zebrafish pretreated with pesticides by a new near-infrared fluorescence off-on probe. *J Agric Food Chem* 2017;65(20):4209–15.
- [19] Jin Q, Feng L, Wang DD, Dai ZR, Wang P, Zou LW, et al. A two-photon ratiometric fluorescent probe for imaging carboxylesterase 2 in living cells and tissues. *ACS Appl Mater Interfaces* 2015;7(51):28474–81.
- [20] Grognum J, Wahler D, Nyfeler E, Reymond JL. Universal chromogenic substrates for lipases and esterases. *Tetrahedron Asymmetry* 2004;15(18):2981–9.
- [21] Weder JKP, Kaiser KP. Fluorogenic substrates for hydrolase detection following electrophoresis. *J Chromatogr A* 1995;698(1–2):181–201.
- [22] Snellman EA, Colwell RR. Transesterification activity of a novel lipase from *Acinetobacter venetianus* RAG-1. *Antonie Leeuwenhoek* 2008;94(4):621–5.
- [23] Hu J, Cheng K, Wu Q, Ding D, Li C, Li Z. A dual fluorogenic and F-19 NMR probe for the detection of esterase activity. *Mater Chem Front* 2018;2(6):1201–6.
- [24] Chen P, He CA. A general strategy to convert the MerR family proteins into highly sensitive and selective fluorescent biosensors for metal ions. *J Am Chem Soc* 2004;126(3):728–9.
- [25] Au-Yeung HY, Chan J, Chantarojsiri T, Chang CJ. Molecular imaging of labile Iron (II) pools in living cells with a turn-on fluorescent probe. *J Am Chem Soc* 2013;135(40):15165–73.
- [26] Li M, Zhai C, Wang S, Huang W, Liu Y, Li Z. Detection of carboxylesterase by a novel hydrosoluble near-infrared fluorescence probe. *RSC Adv* 2019;9(69):40689–93.
- [27] Tallman KR, Beatty KE. Far-red fluorogenic probes for esterase and lipase detection. *Chembiochem* 2015;16(1):70–5.
- [28] Wang K, Kong Q, Chen X, Yoon J, Swamy KMK, Wang F. A bifunctional rhodamine derivative as chemosensor for recognizing Cu^{2+} and Hg^{2+} ions via different spectra. *Chin Chem Lett* 2020;31(5):1087–90.
- [29] Zhang Z, Wang F, Chen X. Recent advances in the development of polydiacetylene-based biosensors. *Chin Chem Lett* 2019;30(10):1745–57.
- [30] Mao Y, Ma M, Wei P, Zhang P, Liu L, Guan T, et al. A sensitive and rapid "off-on" fluorescent probe for the detection of esterase and its application in evaluating cell status and discrimination of living cells and dead cells. *Analyst* 2020;145(4):1408–13.
- [31] Shen T, Zang S, Shu W, Nie L, Jing J, Zhang X. A ratiometric fluorescent probe for mitochondrial esterase specific detection in living cells. *Dyes Pigments* 2020;178:108345–51.
- [32] Wu L, Yang SH, Xiong H, Yang JQ, Guo J, Yang WC, et al. Nonpeptide-based small-molecule probe for fluorogenic and chromogenic detection of chymotrypsin. *Anal Chem* 2017;89(6):3687–93.
- [33] Oe M, Miki K, Ohe K. An enzyme-triggered turn-on fluorescent probe based on carboxylate-induced detachment of a fluorescence quencher. *Org Biomol Chem* 2020;18(42):8620–4.
- [34] Wang K, Xi D, Liu C, Chen Y, Gu H, Jiang L, et al. A ratiometric benzothiazole-based fluorescence probe for selectively recognizing HClO and its practical applications. *Chin Chem Lett* 2020;31(11):2955–9.
- [35] Li J, Chen Y, Chen T, Qiang J, Zhang Z, Wei T, et al. A benzothiazole-based fluorescent probe for efficient detection and discrimination of Zn^{2+} and Cd^{2+} , using cysteine as an auxiliary reagent. *Sens Actuators, B* 2018;268:446–55.
- [36] Ren H, Huo F, Zhang Y, Zhao S, Yin C. An NIR ESIPT-based fluorescent probe with large Stokes shift for specific detection of Cys and its bioimaging in cells and mice. *Sens Actuators, B* 2020;319:128248–55.
- [37] Wei X, Wu Q, Feng Y, Chen M, Zhang S, Chen M, et al. Off-on fluorogenic substrate harnessing ESIPT and AIE features for in situ and long-term tracking of beta-glucuronidase in *Escherichia coli*. *Sens Actuators, B* 2020;304:127242–9.
- [38] Chen Y, Wei T, Zhang Z, Chen T, Li J, Qiang J, et al. A benzothiazole-based fluorescent probe for ratiometric detection of Al^{3+} in aqueous medium and living cells. *Ind Eng Chem Res* 2017;56(43):12267–75.
- [39] Chang C, Wang F, Wei T, Chen X. Benzothiazole-based fluorescent sensor for ratiometric detection of Zn(II) ions and secondary sensing PPI and its applications for biological imaging and PPase catalysis assays. *Ind Eng Chem Res* 2017;56(31):8797–805.
- [40] Li K, Feng Q, Niu G, Zhang W, Li Y, Kang M, et al. Benzothiazole-based AIEgen with tunable excited-state intramolecular proton transfer and restricted intramolecular rotation processes for highly sensitive physiological pH sensing. *ACS Sens* 2018;3(5):920–8.
- [41] Chen Y, Fang Y, Gu H, Qiang J, Li H, Fan J, et al. Color-tunable and ESIPT-inspired solid fluorophores based on benzothiazole derivatives: aggregation-induced emission, strong solvatochromic effect, and white light emission. *ACS Appl Mater Interfaces* 2020;12(49):55094–106.
- [42] Smaga LP, Pino NW, Ibarra GE, Krishnamurthy V, Chan J. A photoactivatable formaldehyde donor with fluorescence monitoring reveals threshold to arrest cell migration. *J Am Chem Soc* 2020;142(2):680–4.
- [43] Chen Y, Wei T, Zhang Z, Zhang W, Lv J, Chen T, et al. A mitochondria-targeted fluorescent probe for ratiometric detection of hypochlorite in living cells. *Chin Chem Lett* 2017;28(10):1957–60.
- [44] Yoon Y, Jo S, Park SJ, Kim HM, Kim D, Lee TS. Unusual fluorescence of o-phenylazonaphthol derivatives with aggregation-induced emission and their use in two-photon cell imaging. *Chem Commun* 2019;55(47):6747–50.